An analytical model for ballistic diode based on asymmetric geometry

Peng Zhang[a] and Derek M. H. Hung
Department of Nuclear Engineering and Radiological Sciences, University of Michigan, Ann Arbor, Michigan 48109-2104, USA

(Received 4 March 2014; accepted 8 May 2014; published online 27 May 2014)

This paper presents an analytical model which calculates the current rectification of an asymmetric two-dimensional ballistic constriction structure in a classical treatment. Such a ballistic diode eliminates the use of p-n junctions or electrodes of dissimilar materials. We show the conditions at which the *I-V* asymmetry may be maximized for various aspect ratios. The analytic theory is verified by Monte Carlo simulations. © *2014 AIP Publishing LLC*. [http://dx.doi.org/10.1063/1.4878975]

I. INTRODUCTION

A diode is a two-terminal electronic component with an asymmetric charge transfer characteristic, with low resistance to current flow in one direction, and high resistance in the opposite direction. This unidirectional behavior offers the fundamental function of signal rectification. A diode is typically implemented by p-n junctions with semiconductors of different doping. Rectification can also be achieved by Schottky contacts between metal and semiconductor. In the miniaturization of these diodes, it usually requires multiple metallic electrodes of dissimilar materials,[1–6] which bring many challenges to the nanolithography technology. Parasitic effects, such as undesired doping and contact resistance, may also be introduced to the junction by the metallic electrodes.[7–10]

It is thus important to seek different mechanisms to give signal rectification. Current rectification based on geometric effects has recently attracted considerable attentions.[6,11–17] Geometrically induced rectification in two-dimensional (2D) ballistic nano-devices is studied quantum mechanically by using Shrodinger and Dirac equations.[11] The asymmetric *I-V* behaviors of a graphene based geometric diode have also been demonstrated by Monte Carlo simulations using the Drude model,[15] as well as by experiments.[14,15] However, there is still a lack of analytic scaling to systematically guide and optimize the geometric design of such devices.

In this paper, we analytically study the current rectification of a 2D asymmetric ballistic constriction (Fig. 1). Following Sharvin[18] and Wexler,[19] we study the ballistic charge transport by using the analogy to dilute gas kinetics (where the mean free path of particles $\geq$ the size of hole on the container wall).[20] We found that there is an optimal condition at which the *I-V* asymmetry is maximized. Our calculations are verified by Monte Carlo simulations (Figs. 3–5), including the effects of a general drift velocity.

II. THE MODEL

Consider a 2D funnel-shaped constriction region between two bulk conductors, as shown in Fig. 1. It is assumed that the charge motion inside the contact region is ballistic. This may be realized if the dimensions of the constriction region, especially the smallest dimension a (Fig. 1), are close to or smaller than the mean-free-path length of the charge carriers in the material.[15,18,20] The charges are assumed to be reflected specularly at the edges of the device.[14,15] The charge carriers inside the circuit may have a general 2D velocity distribution $v_t(\theta)$, where θ is the angle of the velocity and v_t is the magnitude of the velocity at angle θ (Fig. 1). The current entering AB can be expressed as $I_{AB} = qN < v_\perp > \times 2d$, where q (assumed >0 throughout this paper for simplicity) is the charge of a single carrier, N is the number density of the charge carriers, d is the half-width of AB, and

$$< v_\perp > = \frac{\int_{-\pi/2}^{\pi/2} v_t(\theta)\cos\theta\, d\theta}{\int_{-\pi}^{\pi} d\theta} = \frac{1}{2\pi}\int_{-\pi/2}^{\pi/2} v_t(\theta)\cos\theta\, d\theta, \quad (1)$$

which is the average velocity of the charges entering AB from the left. The probability f_1 that the charge carriers at AB can be transported to exit CD is

$$f_1 = \sum_{m=0}^{M} F_m, \quad (2a)$$

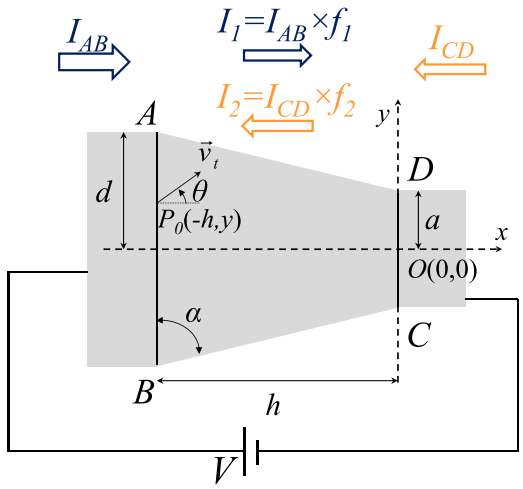

FIG. 1. 2D funnel-shaped ballistic diode. Current entering the interface AB (CD) is I_{AB} (I_{CD}), the probability for charge carriers at AB(CD) that can be transported to CD(AB) is f_1 (f_2), so that the current transported from AB(CD) to CD(AB) is $I_1 = I_{AB} \times f_1$ ($I_2 = I_{CD} \times f_2$).

[a]Electronic mail: umpeng@umich.edu

$$F_m = \frac{2\int_{y_m^{\min}}^{y_m^{\max}}\int_{\theta_m^{\min}(y)}^{\theta_m^{\max}(y)} v_t(\theta)d\theta\,dy}{\int_{-d}^{d}\int_{-\pi/2}^{\pi/2} v_t(\theta)d\theta\,dy} = \frac{\int_{y_m^{\min}}^{y_m^{\max}}\int_{\theta_{\min}(y)}^{\theta_{\max}(y)} v_t(\theta)d\theta\,dy}{d\int_{-\pi/2}^{\pi/2} v_t(\theta)d\theta}, \tag{2b}$$

where F_m is the probability of charge carriers exiting CD from AB after experiencing m reflections with the edges AD and/or BC, and M is the maximum possible reflections that a charge carrier may experience before exiting CD. In Eq. (2b), $y_m^{\min(\max)}$ is the lowest (highest) location of charge carriers on AB that are able to exit CD after m reflections with the two side edges AD and/or BC, and $\theta_m^{\min(\max)}(y)$ is the minimum (maximum) angle of the velocity for a charge carrier located at $P_0(-h, y)$ that is able to exit CD after m reflections (Fig. 1).

The parameters $y_m^{\min(\max)}$, $\theta_m^{\min(\max)}(y)$, and M may be determined easily from the mirror image geometries of the region ABCD, as shown in Fig. 2. Each trapezoid is the mirror image of its neighbor with their shared side as the axis of symmetry. Consider a charge carrier originated at point $P_0(-h, y)$. Its transport to exit CD after m reflections is equivalent to the direct transport to CD from its image point P_m, with $m = 0, 1, 2$. Thus, any charge carriers on AB reflecting once from AD to exit CD may be evaluated from the direct transport of charge carriers from AB's first mirror image A_1A_2 to exit CD (note the overlap of point A and A_1); reflecting twice (BC then AD) to exit CD may be evaluated from the direct transport from A_2A_3 to CD; etc. It is found that

$$y_m^{\min} = \begin{cases} -d, & 0 \le m < M \text{ or } m = M \text{ (even)}, \\ d + x_{A_M}/|\sin 2M\alpha|, & m = M \text{ (odd)}, \end{cases}$$
$$y_m^{\max} = \begin{cases} d, & 0 \le m < M \text{ or } m = M \text{ (odd)}, \\ -d - x_{A_M}/|\sin 2M\alpha|, & m = M \text{ (even)}, \end{cases} \tag{3}$$

$$\theta_m^{\min(\max)}(y) = \begin{cases} \tan^{-1}\left(\dfrac{-y \mp a}{h}\right), & m = 0, \\ (-1)^m\left(m(\pi - 2\alpha) + \tan^{-1}\dfrac{-|\sin 2m\alpha|\cot 2m\alpha\left(d + (-1)^m y\right) + y_{A_m} \pm (-1)^m a}{x_{A_m} + |\sin 2m\alpha|\left(d + (-1)^m y\right)}\right), & 1 \le m \le M, \end{cases} \tag{4}$$

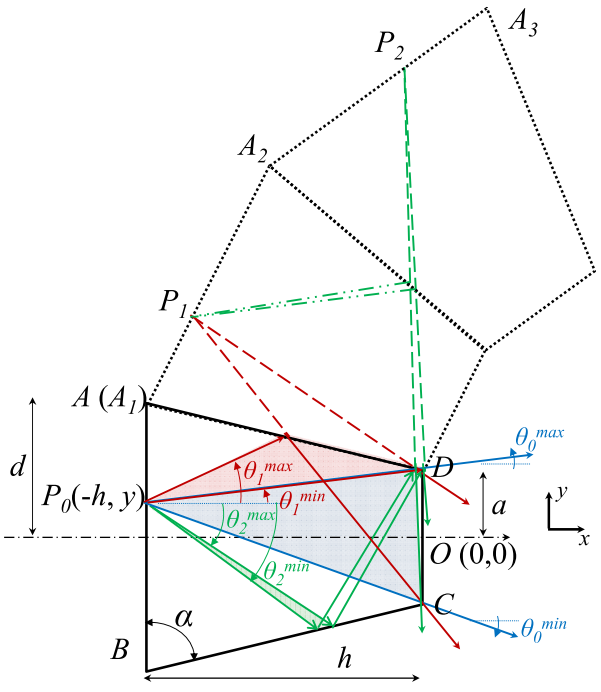

FIG. 2. Mirror images for the tapering region ABCD of Fig. 1. Charges at point P_0 may exit CD through processes: (1) direct transport, spanning angle from $\theta_0^{\min}$ to $\theta_0^{\max}$ (blue); (2) reflecting once from AD, spanning angle from $\theta_1^{\min}$ to $\theta_1^{\max}$ (red); or (3) reflecting twice from BC then AD, spanning angle from $\theta_2^{\min}$ to $\theta_2^{\max}$ (green); etc. $\theta_1^{\min}$ to $\theta_1^{\max}$ in process (2) is obtained by considering the direct transport of charges from P_0's mirror image P_1; $\theta_2^{\min}$ to $\theta_2^{\max}$ in process (3) is obtained by the direct transport from the mirror image point P_2. Other possible processes (e.g., reflecting from AD then BC) are not shown.

where the superscript "min(max)" corresponds to the top (bottom) sign of the $\pm$ and $\mp$ signs, all the dimensions are defined in Fig. 2, and (x_{A_m}, y_{Am}) are the coordinates of the outer corners, A_m, with $(x_{A_1}, y_{A_1}) = (-h, d)$, and $(x_{A_m}, y_{A_m}) = (x_{A_{m-1}} - 2d\sin[(m-1)(2\alpha - \pi)],\ y_{A_{m-1}} + 2d\cos[(m-1)(2\alpha - \pi)])$, for $m > 1$. The final $m = M$ is reached (i.e., maximum possible reflections before exiting from CD) when $x_{A_M} < 0$ and $x_{AM+1} > 0$. The factor of 2 in the first expression of Eq. (2b) counts for the reflections from the mirror images in the negative half plane of the coordinates (not shown) in Fig. 2.

For a given constriction geometry of a, h, α (note $d = a + h/\tan\alpha$), and a given velocity distribution of the charge carriers $v_t(\theta)$, the current that can be transported from left to right (i.e., AB to CD) is $I_1 = I_{AB} \times f_1$, where I_{AB} and f_1 are obtained from Eqs. (1) and (2), respectively. Similarly, the current I_2 that can be transported from right to left (i.e., CD to AB) is

$$I_2 = I_{CD} \times f_2 = I_{CD} = -\frac{qNa}{\pi}\int_{-\pi/2}^{\pi/2} v_t(\theta)\cos\theta\,d\theta, \tag{5}$$

since the probability of charge carriers originating from CD to exit AB is $f_2 = 1$. In Eq. (5), the integration is carried out for the angles with negative $\cos\theta$ only. The net current would be $I_{net} = I_1 - I_2$ (Fig. 1).

III. RESULTS AND DISCUSSION

Consider the zero external bias ($V = 0$) case first. Under zero bias, the charge carriers inside the circuit are assumed

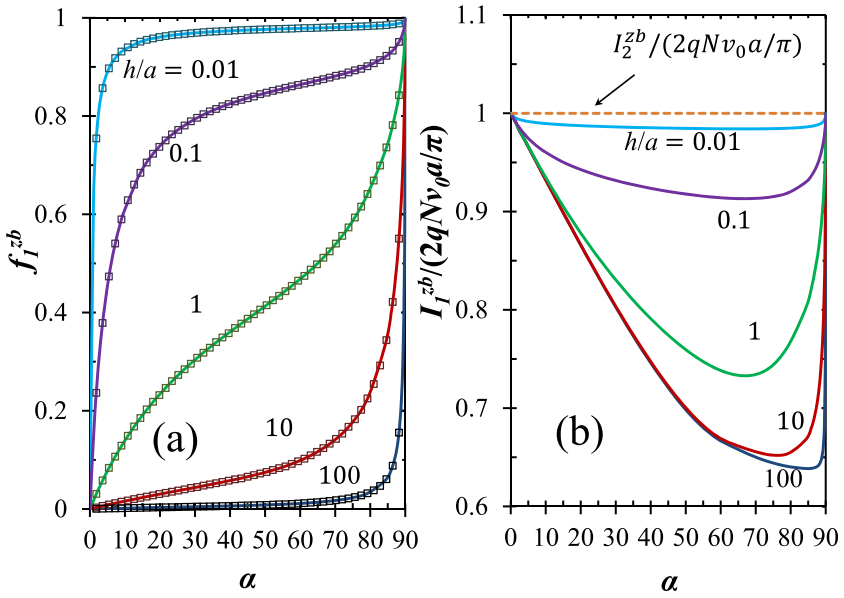

FIG. 3. Zero-bias case, charges with isotropic initial velocity: (a) the probability of charge carriers transporting from AB to CD, f_1^{zb}, and (b) the current from AB to CD, $I_1^{zb} = I_{AB}^{zb} \times f_1^{zb}$ (normalized to $2qNv_0a/\pi$), as a function of α for various h/a. Dashed line in (b) is for the current from CD to AB, $I_2^{zb} = 2qNv_0a/\pi$. Symbols are for Monte Carlo simulations.

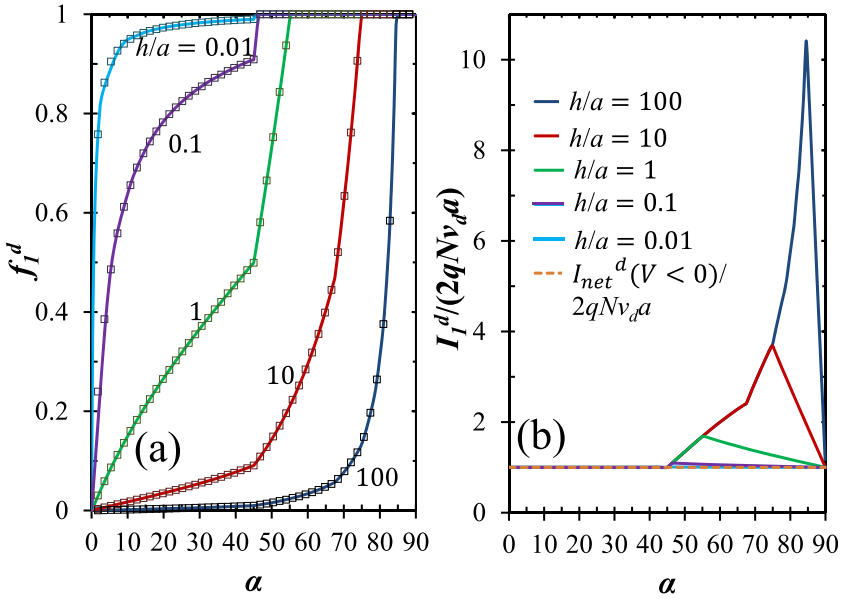

FIG. 4. Drift-only case: (a) the probability of charge carriers transporting from AB to CD, f_1^d, and (b), the current from AB to CD, $I_1^d = I_{AB}^d \times f_1^d$ (normalized to $2qNv_da$), as a function of α for various h/a. Note that $I_{net}^d(V > 0) = I_1^d - I_2^d = I_1^d$. Dashed line in (b) is for the net current from CD to AB when drift velocity pointing to the left, i.e., $I_{net}^d(V < 0) = 2qNv_da$. Symbols are for Monte Carlo simulations.

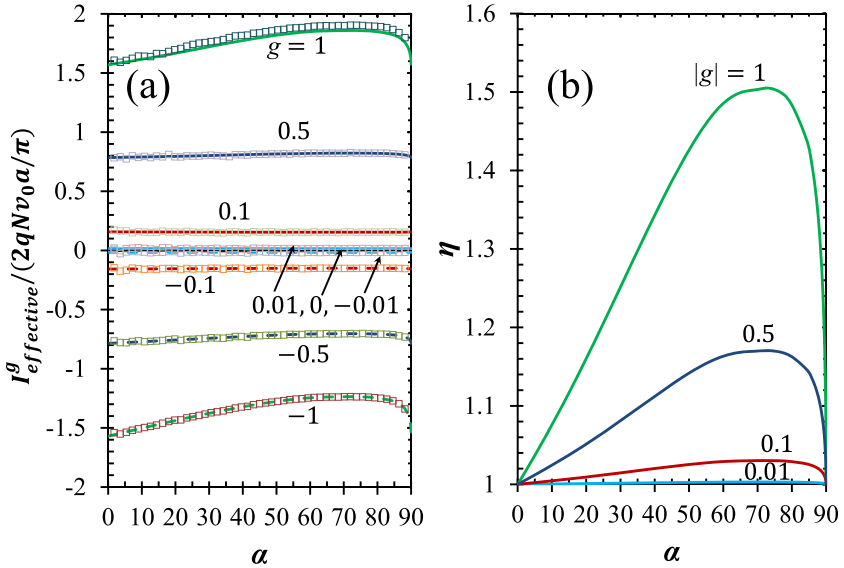

FIG. 5. (a) The effective net current $I_{effective}^g = I_{net}^g - I_{net}^{zb}$ (normalized to $2qNv_0a/\pi$) under various bias induced $g = v_d/v_0$ ratios; (b) the I-V asymmetry, $\eta = I_{effective}^g(V > 0)/(-I_{effective}^g(V < 0))$, as a function of α.

to move randomly with an isotropic distribution of initial velocity, with a constant magnitude of $v_t(\theta) = v_0$. We use superscript "zb" to denote quantities for the zero bias case. From Eq. (1), the current entering AB is

$$I_{AB}^{zb} = 2qN\frac{v_0}{\pi}d. \tag{6}$$

The probability of charge carriers transporting from AB to CD in Eq. (2) is simplified to be

$$f_1^{zb} = \frac{1}{\pi d}\sum_{m=0}^{M}\int_{y_m^{\min}}^{y_m^{\max}}\int_{\theta_{\min}(y)}^{\theta_{\max}(y)} d\theta\, dy, \tag{7}$$

which is plotted in Fig. 3(a) as a function of α for various h/a. For a given h/a, f_1^{zb} increases as α increases. For a given α, f_1^{zb} decreases as h/a increases. In the limit of $\alpha \to 0$, $f_1^{zb}(\alpha = 0) = a/d = 1/[1 + (h/a)/\tan\alpha] \to 0$. In the opposite limit of $\alpha = \pi/2$, the region ABCD in Fig. 1 becomes rectangular, which allows all the charge carriers entering AB to transport to CD, resulting $f_1^{zb}(\alpha = \pi/2) = 1$, since specular reflections from AD and BC are assumed so that all the charges entering AB are able to exit from CD. Monte Carlo simulations are performed to verify the calculations. Excellent agreement between the analytical results and Monte Carlo simulations are obtained, as seen from Fig. 3(a).

From Eqs. (6) and (7), the current that can be transported from AB to CD is calculated as $I_1^{zb} = I_{AB}^{zb} \times f_1^{zb}$, which is plotted in Fig. 3(b). Similarly, from Eq. (5), we obtain the current that can be transported from right to left (i.e., CD to AB) as $I_2^{zb} = 2qNv_0a/\pi$, which is also plotted in Fig. 3(b). There is a non-zero net current $I_{net}^{zb} = I_1^{zb} - I_2^{zb}$ under zero bias.[21] However, it is surprising that the current flowing from AB to CD is *smaller* than that of from CD to AB, $I_1^{zb} < I_2^{zb}$, under zero external bias, with charge carriers having isotropic velocity distribution. In this case, the tapering edges of the constriction region result in more blockade of current so that the preferable direction of charge flow is from right to left, i.e., CD to AB. That is, the net current inside the constriction region is from right to left. Note that in both the limits of $\alpha \to 0$ and $\alpha \to \pi/2$, we have $I_1^{zb} \to I_2^{zb}$, where the contact region has little influence on the charge transport. It is clear from Fig. 3(b) that there is a maximum zero-bias net current $I_{net}^{zb} = I_1^{zb} - I_2^{zb}$ for a given h/a. The value of α at which I_{net}^{zb} is maximized increases with h/a.

On applying an external bias, an average drift velocity v_d will be induced to the charge carriers. The resulting velocity distribution would be the superposition of the initial isotropic velocity $v_0(\theta)$ and the bias-induced drift velocity $v_d(\theta = 0)$, which is assumed to be proportional to the applied bias V. Depending on the direction of bias, the magnitude of the net current is expected to vary.

For simplicity, we first consider the ideal case where all charge carriers have only a single drift velocity v_d ($\theta = 0$). We use superscript "d" to denote quantities for this "drift-only" case. When the bias $V > 0$ (the potential in the left is higher than in the right in Fig. 1), we have $v_d > 0$, i.e., pointing to the right, assuming positive carrier charge ($q > 0$). The current transport from AB to CD is $I_1^d = I_{AB}^d \times f_1^d$, where $I_{AB}^d = 2qNv_d d$ and f_1^d is the probability of charges entering AB to be able to exit CD, shown in Fig. 4(a). f_1^d is calculated similarly by using the mirror image method (cf. Fig. 2). Similar to the zero-bias case, f_1^d increases with α, for a given h/a. f_1^d decreases as h/a increases, for a given α. However, f_1^d increases much more rapidly with α than f_1^{zb} in the zero-bias case and saturates at 1 before α reaches $\pi/2$. The current transport from AB to CD I_1^d is plotted in Fig. 4(b), showing clearly a maximum current at certain α for a given h/a. The value of α for the maximum current I_1^d increases as h/a increases. Note that the current transport from CD to AB is $I_2^d = 0$; thus, the net current flowing from AB to CD is $I_{net}^d(V > 0) = I_1^d - I_2^d = I_1^d$. Also note the excellent agreement between the results from the analytical calculation and the Monte Carlo simulation. In contrast, when $v_d < 0$, i.e., pointing to the left, the net current from CD to AB is $I_{net}^d(V < 0) = 2qNv_d a$, which is independent of α. Therefore, for the case with drift velocity only, significant asymmetric I-V characteristics are realized, with carriers flowing preferably in the forward direction when the structure in Fig. 1 is forward biased ($V > 0$).

In general, the velocity distribution of the charge carriers is a superposition of the initial isotropic velocity $v_0(\theta)$ (a circle with its center at the origin and radius of v_0 in the velocity space) and the bias-induced drift velocity $v_d(\theta = 0)$, the circle in the velocity space would be shifted to the right with its center at $(v_d, 0)$, we have

$$\begin{aligned} &v_t(\theta) = v_0\sqrt{1 + g^2 + 2g\cos\theta_0}; \\ &\sin\theta = \sin\theta_0/\sqrt{1 + g^2 + 2g\cos\theta_0}; \quad -\pi < \theta_0 \le \pi, \end{aligned} \tag{8}$$

where θ_0 is the corresponding angle of θ before the shifting, and $g = v_d/v_0$ is the drift-to-isotropic velocity ratio. Note that Eq. (8) gives $v_t(\theta) = v_0$ when $g = 0$, as expected. We use superscript "g" to denote quantities for the case with the general velocity distribution, Eq. (8). Equation (8) is used together with Eqs. (1)–(5) to obtain the current components I_1^g and I_2^g in various g ratios. The net current would be $I_{net}^g = I_1^g - I_2^g$. As shown earlier, there is a zero-bias current I_{net}^{zb} for $v_d = 0$, or $V = 0$. Thus, it is meaningful to obtain the effective current, $I_{effective}^g = I_{net}^g - I_{net}^{zb}$, which is the change of current due to the applied bias (velocity distribution of Eq. (8)) from the zero-bias case (isotropic velocity distribution). $I_{effective}^g$ is plotted as a function of α for various g in Fig. 5(a), for the special case of $h/a = 5$. It is found that $I_{effective}^g$ increases as g increases. However, the α for the maximum current is insensitive to the applied bias, for a given value of h/a. The I-V asymmetry, measured by $\eta = I_{effective}^g(V > 0)/(-I_{effective}^{-g}(V < 0))$, increases as $|g|$ (or V) increases, as shown in Fig. 5(b). Since the asymmetry η is insensitive to the applied bias, the ideal case of drift velocity only (Fig. 4) may be used to estimate the optimal geometry to maximize the I-V asymmetry.

IV. CONCLUSION

In summary, we have studied the I-V asymmetry as a function of tapered angles and dimensional ratios for a geometrically induced diode based on ballistic transport. The

conditions for maximum *I-V* asymmetry are determined, which may be used to optimize the design of such a junction-less diode. Such a device may be realized using materials with long charge mean free path, such as graphene.[11,12,14,15,22] The study may also be considered an extension of the basic symmetric Sharvin contact.[18,19]

ACKNOWLEDGMENTS

We thank Professor Y. Y. Lau for support and encouragement, and Professor Martin Peckerar and Professor Ronald Gilgenbach for stressing to us the importance of this problem. We would like to thank Y. X. Liu for useful discussions. This work was supported by AFOSR Grant No. FA9550-09-1-0662, and L-3 Communications Electron Devices Division.

[1]G. D. J. Smit, S. Rogge, and T. M. Klapwijk, "Scaling of nano-Schottky-diodes," Appl. Phys. Lett. **81**, 3852 (2002).
[2]J. R. Williams, L. Dicarlo, and C. M. Marcus, "Quantum hall effect in a gate-controlled p–n junction of graphene," Science **317**, 638 (2007).
[3]J. G. Simmons, "Potential barriers and emission limited current flow between closely spaced parallel metal electrodes," J. Appl. Phys. **35**, 2472 (1964).
[4]M. H. Yang, K. B. Teo, W. Milne, and D. Hasko, "Carbon nanotube Schottky diode and directionally depend field-effect transistor using asymmetric contacts," Appl. Phys. Lett. **87**, 253116 (2005).
[5]C. Lu, L. An, Q. Fu, J. Liu, H. Zhang, and J. Murduck, "Schottky diodes from asymmetric metal–nanotube contacts," Appl. Phys. Lett. **88**, 133501 (2006).
[6]C. Balocco, S. R. Kasjoo, X. F. Lu, L. Q. Zhang, Y. Alimi, S. Winnerl, and A. M. Song, "Room temperature of a unipolar nanodiode at terahertz frequencies," Appl. Phys. Lett. **98**, 223501 (2011).
[7]G. Giovannetti, *et al*., "Doping graphene with metal contacts," Phys. Rev. Lett. **101**, 026803 (2008).
[8]F. Xia, V. Perebeinos, Y. Lin, Y. Wu, and P. Avouris, "The origins and limits of metal-graphene junction resistance," Nat. Nanotechnol. **6**, 179–184 (2011).
[9]P. Zhang and Y. Y. Lau, "Scaling laws for electrical contact resistance with dissimilar materials," J. Appl. Phys. **108**, 044914 (2010).
[10]P. Zhang, D. Hung, and Y. Y. Lau, "Current flow in a 3-terminal thin film contact with dissimilar materials and general geometric aspect ratios," J. Phys. D: Appl. Phys. **46**, 065502 (2013); Corrigendum, *ibid.* **46**, 209501 (2013).
[11]D. Dragoman and M. Dragoman, "Geometrically induced rectification in two-dimensional ballistic nanodevices," J. Phys. D: Appl. Phys. **46**, 055306 (2013).
[12]D. Dragoman, M. Dragoman, and R. Plana, "Graphene-based ultrafast diode," J. Appl. Phys. **108**, 084316 (2010).
[13]K. Choi, G. Ryu, F. Yesilkoy, A. Chryssis, N. Goldsman, M. Dagenais, and M. Peckerar, "Geometry enhanced asymmetric rectifying tunneling diodes," J. Vac. Sci. Technol. B **28**, C6O50 (2010).
[14]G. Moddel, Z. Zhu, S. Grover, and S. Joshi, "Ultra high speed graphene diode with reversible polarity," Solid State Commun. **152**, 1842 (2012).
[15]Z. Zhu, S. Joshi, S. Grover, and G. Moddel, "Graphene geometric diodes for terahertz rectennas," J. Phys. D: Appl. Phys. **46**, 185101 (2013).
[16]Y. B. Zhu, P. Zhang, A. Valfells, L. K. Ang, and Y. Y. Lau, "Novel scaling laws for the Langmuir-Blodgett solutions in cylindrical and spherical diodes," Phys. Rev. Lett. **110**, 265007 (2013).
[17]M. Ali *et al*., "Nanoparticle-induced rectification in a single cylindrical nanopore: Net currents from zero time-average potentials," Appl. Phys. Lett. **104**, 043703 (2014).
[18]Y. V. Sharvin, "A possible method for studying fermi surfaces," Sov. Phys.-JETP **21**, 655 (1965).
[19]G. Wexler, "The size effect and the non-local Boltzmann transport equation in orifice and disk geometry," Proc. Phys. Soc. **89**, 927 (1966).
[20]R. D. Present, *Kinetic Theory of Gases* (McGraw-Hill, New York, 1958), p. 22.
[21]S. Datta and M. P. Anantram, "Steady-state transport in mesoscopic systems illuminated by alternating fields," Phys. Rev. B **45**, 13761 (1992).
[22]J. Baringhaus, M. Ruan, F. Edler, A. Tejeda, M. Sicot, A. Taleb-Ibrahimi, A. Li, Z. Jiang, E. H. Conrad, C. Berger, C. Tegenkamp, and W. A. de Heer, "Exceptional ballistic transport in epitaxial grapheme nanoribbons," Nature **506**, 349–354 (2014).